Effects of weaving parameters on the properties of completely biological tissue-engineered vascular grafts

Gaëtan Roudier, Marie Hourques, Nicolas da Silva, Maude Gluais, Emmanuel Binyet, Jean-Marc Olive, Nicolas L'heureux

PAPER • **OPEN ACCESS**

Effects of weaving parameters on the properties of completely biological tissue-engineered vascular grafts

To cite this article: Gaëtan Roudier *et al* 2024 *Biofabrication* **16** 015015

Biofabrication

PAPER

Effects of weaving parameters on the properties of completely biological tissue-engineered vascular grafts

Gaëtan Roudier[1], Marie Hourques[1], Nicolas Da Silva[1], Maude Gluais[1], Emmanuel Binyet[2], Jean-Marc Olive[2] and Nicolas L'Heureux[1,*]

[1] University Bordeaux, INSERM, Laboratory for the Bioengineering of Tissues—BioTis, UMR 1026, F-33076 Bordeaux, France
[2] University Bordeaux, CNRS, UMR 5295, I2M, F-33405 Talence, France
* Author to whom any correspondence should be addressed.

E-mail: nicolas.lheureux@inserm.fr

OPEN ACCESS

RECEIVED
12 July 2023

REVISED
24 October 2023

ACCEPTED FOR PUBLICATION
16 November 2023

PUBLISHED
24 November 2023

Keywords: extracellular matrix, vascular graft, tissue engineering, biological textiles, weaving parameters, mechanical properties

Supplementary material for this article is available online

Abstract

Tissue-engineered vascular grafts (TEVGs) made of human textiles have been recently introduced and offer remarkable biocompatibility as well as tunable mechanical properties. The approach combines the use of cell-assembled extracellular matrix (CAM) threads, produced by cultured cells *in vitro*, with weaving, a versatile assembly method that gives fine control over graft properties. Herein, we investigated how production parameters can modify the geometrical and mechanical properties of TEVGs to better match that of native blood vessels in order to provide long-term patency. Our goals were to decrease the mechanical strength and the luminal surface profile of our first generation of woven TEVGs, while maintaining low transmural permeability and good suture retention strength. Different TEVGs were produced by varying CAM sheet strength as well as weaving parameters such as warp count, weft ribbons width, and weft tension. An optimized design reduced the burst pressure by 35%, wall thickness by 38% and increased compliance by 269%. The improved TEVG had properties closer to that of native blood vessels, with a burst pressure of 3492 mmHg, a wall thickness of 0.69 mm, and a compliance of 4.8%/100 mmHg, while keeping excellent suture retention strength (4.7 N) and low transmural permeability (24 $ml \cdot min^{-1} \cdot cm^{-2}$). Moreover, the new design reduced the luminal surface profile by 48% and utilized 47% less CAM. With a comparable design, the use of decellularized CAM threads, instead of devitalized ones, led to TEVGs with much more permeable walls and higher burst pressure. The next step is to implant this optimized graft in an allogeneic sheep model of arteriovenous shunt to assess its *in vivo* remodeling and performance.

1. Introduction

Small to mid-diameter vascular grafts are implanted daily by surgeons, whether it is for lower limb revascularization, coronary bypasses, or as arteriovenous shunts. Autologous blood vessels are the gold standard but these conduits have limited availability and are not always in the best of conditions. While synthetic prosthesis are available 'off-the-shelf', they are prone to thrombosis, intimal hyperplasia, and infections [1–3]. More than 30 years ago, Weinberg and Bell paved the way for the development of tissue-engineered vascular grafts (TEVGs) with the first biological blood vessel model [4]. Since then, several strategies have emerged to produce the best TEVG, based on scaffolds made of synthetic and natural materials [5, 6]. Biological scaffolds made from mammalian extracellular matrix (ECM) have been very successful in tissue engineering applications [7]. Indeed, ECM is present in every tissue and guides cellular responses, tissue healing and regeneration. However, purified proteins isolated from animal or cadavers do not have a physiological arrangement, thus are rapidly degraded when implanted *in vivo* [8–10]. ECM assembled by cells *in vitro* recreate a more physiological structure and, for this reason, can be the material of choice for tissue engineering that aims to produce a stable structure [11–15]. TEVGs

based on ECM synthesized by cells *in vitro* have been proposed as promising alternatives to synthetic grafts, especially because this is a cell-friendly material that promotes *in vivo* remodeling and avoids infection [11, 16, 17]. L'Heureux *et al* was the first to demonstrate the use of cell-assembled extracellular matrix (CAM) to produce completely biological, implantable, vascular substitutes [18]. These grafts, produced by rolling sheets of CAM to form a biological tube, were successfully implanted in humans [19, 20]. However, while providing successful clinical outcomes, these TEVGs took months to produce, required costly bioreactors, and their mechanical properties were poorly tunable.

A vascular graft must, at least, withstand high pressures, be suturable, and have leak-proof walls to be implantable. To achieve long-term success, a key mechanical property is compliance. Indeed, compliance mismatch with native tissue has been well-established as a cause of intimal hyperplasia and vascular graft failure [21–26]. In addition to those mechanical requirements, the ideal substitute should be easily available and should allow host cells to function normally to fight infections (unlike synthetic materials), to repair damage (e.g. after puncture), or to grow the tissue (e.g. in the case of pediatric application).

Textile technologies allow the production of fabrics with controlled geometrical and mechanical properties. Widely used to produce synthetic vascular substitutes, this approach is increasingly popular for various tissue engineering applications [27, 28]. Recently, our group produced threads from devitalized CAM sheets [29]. These threads have been shown to be stable *in vitro* for 1 year and sterilizable with minimal denaturation [30]. This new shape of the material enables the use of textile approaches to engineer CAM-based products. Among assembly methods, weaving offers the possibility of creating leak-proof walls, which is a critical property for a vascular graft. Our first prototype of woven TEVG had an extremely high burst pressure and suture retention strength. However, such supraphysiological properties were associated with poor compliance, thus creating a mechanical mismatch with native blood vessels. Moreover, the first prototype had thick walls and was not flexible, which made puncturing and suturing the TEVGs difficult [29]. The main objective of this study was to understand the effects of weaving parameters on the properties of the TEVGs in order to correct this mechanical mismatch, while maintaining good suturability and low transmural permeability. A secondary objective was to reduce wall thickness to improve graft handling characteristics. An additional objective was to minimize the surface profile of the lumen of the graft to reduce hemodynamic perturbations. Finally, design improvements were expected to reduce the amount of CAM used to limit TEVG cost.

In this report, we demonstrate how the structural and mechanical properties of these completely biological woven TEVGs can be improved by adapting our material and controlling the assembly parameters. Such data will help to build a toolbox to produce the optimal TEVG to achieve long-term *in vivo* success, but also to produce human textiles with relevant properties for other applications.

2. Materials and methods

2.1. Devitalized CAM sheet production and characterization

CAM sheets were produced as previously described [31]. Sheep skin fibroblasts (SSFs) were isolated from sheep skin biopsies as previously detailed and were seeded in 225 cm^2 flasks at a density of 10^4 cells·cm^{-2}. Cells were cultured for several weeks, depending on the desired strength, in DMEM/F-12 medium (Gibco®, #31331028) supplemented with 10% fetal bovine serum (FBS, Hyclone™ FetalClone III, #AD19958305) and 0.5 mM sodium L-ascorbate (Sigma, #A4034). CAM sheets were also produced in 6-well plates. Media were changed three times a week. Once produced, CAM sheets were quickly rinsed in sterile distilled water and frozen at −80 °C. When needed, sheets were thawed, rinsed in sterile distilled water, and air-dried under the sterile air flow of a biosafety cabinet at room temperature. Dried sheets were stored at −80 °C until needed. Prior to use, CAM was rehydrated in sterile water for at least 1 h and used as devitalized material. A perforation test with a computer-controlled device (Shimadzu Autograph AGS-X series, force transducer 100 N) was done to determine CAM sheet strength. Six-well plate CAM sheets were held by a custom-made device and perforated with a spherical tip mounted with a 9 mm plastic ball at a rate of 20 mm·min^{-1} until rupture. Data were analyzed with Trapezium-X software. Thickness of fully rehydrated CAM sheets were determined with a bi-axial laser micrometer (Xactum, AEROEL).

2.2. Devitalized threads production and characterization

Two sets of threads were produced, the warp (longitudinal threads) and the weft (circumferential thread), as previously described [29].

For warp threads production, thawed CAM sheets were placed in a cutting device. Circular blades were pressed on the sheet and the device was pushed to rotate the blades and cut the CAM to obtain 5 mm wide by 17 cm long ribbons.

For weft production, CAM sheets were thawed and dried on the back of a thin sacrificial plastic sheet with a printed spiral pattern of a desired width. CAM sheets were cut with surgical scissors following the spiral pattern. Using this approach, two long ribbons of approximately 1.5 m can be produced from a single 225 cm^2 sheet. Then, the internal part of one spiral was attached with the external part of the second one and the two ribbons were twisted together at a rate

5 revolutions per centimeter of length using a rotating motorized device in order to produce an elastic thread. Ribbons were then dried under a laminar flow hood, spooled, and stored at −80 °C until needed. Weft was produced from 3 mm, 4 mm and 5 mm wide ribbons.

Thickness or diameter of fully rehydrated threads were determined with a bi-axial laser micrometer (Xactum, AEROEL). Afterwards, threads were put in between the jaws of a tensile test machine (Shimadzu, AGS-X, force sensor 100 N). Threads were pre-loaded at 20 mm min^{-1} until 0.1 N and pulled until breakup at speed of 1% of loaded initial length per second. Samples remained hydrated during the test and the force at failure (N) was recorded.

2.3. CAM decellularization

To produce decellularized woven TEVGs, CAM sheets were decellularized as previously described [32]. Briefly, frozen CAM sheets were thawed in sterile distilled water. The water was then replaced with 120 ml of a decellularization solution composed of 8 mM 3-[(3-cholamidopropyl)dimethylammonio]-1-propanesulfonate (CHAPS), 1000 mM sodium chloride (NaCl), 25 mM ethylenediaminetetraacetic acid (EDTA), and 120 mM sodium hydroxide (NaOH) diluted in 1X phosphate buffered saline (1X PBS, Gibco®, #10010023). CAM sheets were immerged in the solution for 6 h under strong agitation, before being rinsed three times in 1X PBS for 30 min and once in sterile distilled water overnight under agitation. Decellularized CAM sheets were used for threads production as described. To confirm efficient decellularization, rehydrated devitalized and decellularized 5 mm^2 samples of CAM were fixed in a 4% of paraformaldehyde-based solution (Antigenfix, Microm Microtech) for 1 h. After two rinses in 1X PBS, Triton-X 0.1% was added to the samples for 15 min to permeabilize cells membranes. Following three washing steps of 5 min in 1X PBS, 4′,6-diamidino-2-phenylindole (DAPI, 1:1000, D1306, Invitrogen) was applied for 1 h at room temperature. Images were acquired using a confocal microscope (TCS SPE, Leica microsystems).

2.4. DNA quantification

The DNA of devitalized and decellularized CAM sheets was quantitated to validate decellularization. Dry samples were weighed and DNA was extracted and purified with a QIAamp® DNA mini kit (Qiagen, #51304) following manufacturer's instructions. Absorbance was measured with a photometer p330 (Implen) and DNA concentration was reported in ng per mg CAM dry weight.

2.5. TEVG production

TEVGs were woven on a custom-made circular loom, in plain weave and over a 4.2 mm diameter mandrel. The weft (circumferential thread) was inserted between a movable and a fixed set of tensioned warp (longitudinal thread) and then manually tensioned. The movable set of warp was then moved to cross over the manually tensioned weft and the latter was run again between the two sets of warp, and so on to create the woven TEVG. TEVGs were produced to test three levels for each of the 3 assembly variables tested. Warp count (total number of longitudinal threads) was the first variable tested because it is easily controllable and, since these threads are the main component of the vessel, has the highest potential of significantly decreasing the amount of material used. It was decreased from 51, to 43 and 27 threads per vessel. Weft diameter was then evaluated because it can also be well controlled and was expected to most effectively reduce the excessive burst strength of the initial vessel prototype (one of the key objectives of the optimization). It was decreased from 5 mm to 4 and then to 3 mm. In this manual process, thinner ribbons ($\leqslant$2 mm) are more difficult to handle without occasional breakages and, hence, were not included in this initial optimization study. Finally, weft tension was tested because we hypothesized that this variable could improve the compliance of the vessel (a property often considered essential for long-term success). Other assembly variables could be tested (e.g. warp width, warp tension, etc) in further studies but are technically more challenging to address. TEVGs were removed from the mandrel once produced and fully rehydrated before analysis.

2.6. Microcomputed tomography imaging

TEVGs were scanned with microcomputed tomography (μCT) (V|tome|X—S model, General Electric) at a 8 μm resolution (500 ms exposure, 100 kV, 100 μA). Images were used to measure wall thickness, internal diameter and warp width with ImageJ software (National Institute of Health, USA). The lumen surface waviness was measured using a 3D reconstruction of the TEVGs done with ImageJ (1800 cross sections). Briefly, 4 orthogonal longitudinal sections of each TEVG were extracted from the 3D reconstructions. To evaluate the waviness of the luminal surface, the length and height of each 'wave' within each longitudinal section was manually measured and all values were averaged. Hence, the mean wave length (W_L) and the mean wave height (W_h) were reported for each TEVG. The aspect ratio (AR) was determined as the ratio of the mean height over the mean length.

2.7. Transmural permeability

Water permeability testing was adapted from ISO standards (ISO 7198:2016). TEVGs ($n = 3$) were cannulated and pressurized with water at 120 mmHg. The water leaking through the graft material during each of three 1 min trials was collected and transmural permeability was expressed as $ml{\cdot}min^{-1}{\cdot}cm^2$.

2.8. Compliance measurements

Compliance testing was adapted from ISO standards (ISO 7198:2016). TEVGs were cannulated and cannulas were connected to a jig where the distance between the cannulas was fixed at the unpressurized length of the graft. The system was submerged in water and pressurized over the 80–120 mmHg pressure range three times. High resolution digital images (1.4 μm resolution) were recorded to measure the external diameter. The inside diameter and wall thickness of the TEVG at rest were obtained from μCT images. Assuming an incompressible wall, compliance (in %/100 mmHg) was calculated as follows:

$$\%\text{compliance}\ /100\ \text{mmHg} = \frac{\frac{R_{ip2}-R_{ip1}}{R_{pi}}}{p_2 - p_1} \times 10^4$$

where:
$p_1 = 80$ mmHg,
$p_2 = 120$ mmHg,
R_{ipx} = internal radius at pressure x

2.9. Suture retention testing

Suture retention was performed following ISO standards (ISO 7198:2016) as previously described [33]. Suture retention strength was measured with loop of 6/0 polypropylene suture (SMI) traversing the wall at 2 mm from one extremity of the TEVG and pulled at a steady rate of 150 mm min^{-1} with a uniaxial tensile testing device until failure (100 N load cell, Shimadzu Autograph AGS-X series). The maximum force applied was recorded digitally by the software TrapeziumX (Shimadzu). Both extremities of each TEVG were tested.

2.10. Burst pressure measurements

Burst pressure was performed following ISO standards (ISO 7198:2016). The test was done as previously described with some modifications [33]. A thin latex balloon was used in the TEVG to avoid leakage at high pressure. TEVGs were cannulated and slowly pressurized with nitrogen until failure. A digital pressure gauge LEO5 (Keller) with its data acquisition system (Kolibri Desktop, Keller) and a computer were used to record the pressure at a sampling rate of 10 Hz. All ruptures occurred away from the connection to the cannulas. The pressure needed to dilate the balloon to a diameter larger than that of the TEVG (100 mmHg) was negligible compared to the burst pressure.

2.11. Computational fluid dynamics (CFD)

The computed tomography scans of the TEVGs were processed with the open source software MeshLab (www.meshlab.net/) where only the inner surface of the TEVG (lumen) was kept. ANSYS SpaceClaim (ANSYS, Inc.) was used to fill the lumen and thus create the inner volume. The fluid volume was then discretized using the ANSYS Meshing tool. The inlet face was set as a velocity inlet with a constant velocity of 0.168 m s^{-1}. The outlet face was set as a pressure outlet with a gauge pressure of 100 mmHg. The density of the blood was set as 1060 kg m^{-3}, while TEVG wall was set as rigid and static.

The wall shear stress (WSS) was described by:

$$\tau_w = \mu \left(\frac{\partial u}{\partial y}\right)_{y=0} \quad (1)$$

where μ represents the viscosity of the fluid, u the velocity parallel to the wall and y the perpendicular distance to the wall. The incompressible continuity and momentum equations were given according to:

$$\nabla \vec{u} = 0 \quad (2)$$

$$\rho \frac{\partial \vec{u}}{\partial t} + \rho \vec{u} \cdot \nabla \vec{u} = -\nabla p + \nabla \cdot \vec{\vec{\tau}} + \vec{F}. \quad (3)$$

The Quemada viscosity model was used to create a user-defined viscosity in the fluid solver of the commercial software Ansys Fluent (ANSYS, Inc.) [34]. The viscosity μ was expressed as:

$$\mu = \mu_0 \left(1 - 0.5 Hct \cdot k_Q\right)^{-2} \quad (4)$$

where $\mu_0 = 0.001\ 67$ Pa·S and the hematocrit level is $Hct = 0.45$. The influence of the local shear rate $\dot{\gamma}$ and the critical shear rate $\dot{\gamma}_c = 5$ S^{-1} was modeled using the intrinsic viscosity [34]:

$$k_Q = \frac{k_0 + k_\infty (\dot{\gamma}/\dot{\gamma}_c)^{0.5}}{1 + (\dot{\gamma}/\dot{\gamma}_c)^{0.5}} \quad (5)$$

where $k_\infty = 1.5$ and $k_0 = 4$ are the values for infinitely large and vanishing shear rate, respectively.

Ansys Fluent (ANSYS, Inc.) was used to solve the fluid flow equations and compute WSS through the TEVGs.

2.12. Statistical analysis

All statistical analyses were performed with GraphPad Prism, Version 8 (GraphPad Software Inc.). Data are presented as mean ± standard deviation (SD). The normality of the data distribution was checked with a Shapiro–Wilk test. Differences between groups were determined using unpaired t-tests (two tailed) or one-way ANOVA tests with Tukey's multiple comparison test, as specified in the result section. Differences were considered significant for $p < 0.05$.

3. Results

3.1. TEVG fabrication

Figure 1 illustrates the steps involved in TEVG production. Thawed CAM sheets (figure 1(a)) are used to produce warp and weft threads. Warp threads are made from 5 mm wide ribbons of CAM (figures 1(b)–(d)). Weft threads are produced from two long ribbons of CAM twisted together (figures 1(e)–(g)). Two ribbons are used to produce the weft so the thread can better resist weekly repeated

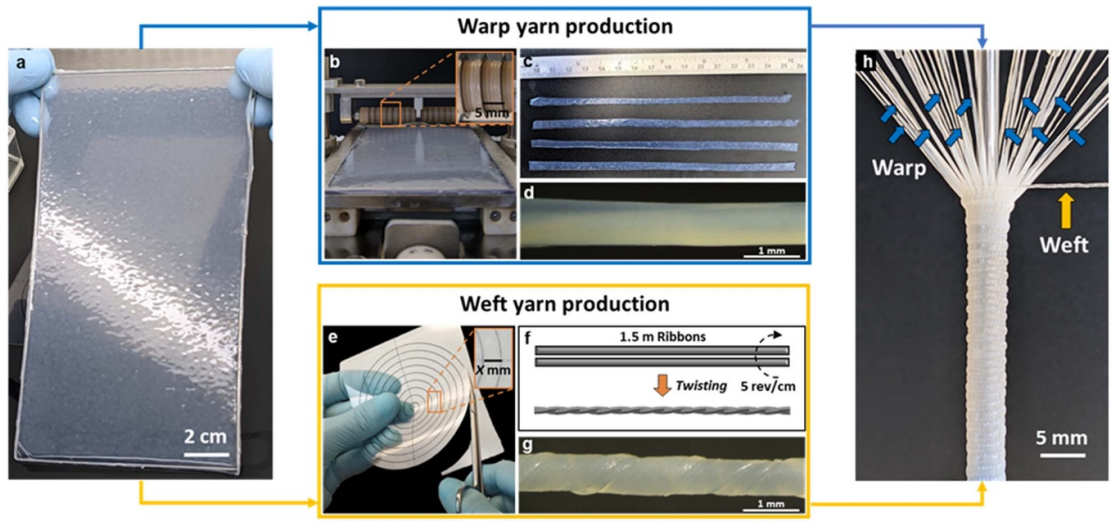

Figure 1. Production of a woven TEVG. (a) Cell-assembled extracellular matrix (CAM) sheets were cut to produce two different types of threads. (b)–(d) The warp was made up of group of 5 mm wide ribbons cut along the long axis of the sheet. Once cut, the ribbons folded onto themselves and looked like threads. (e)–(g) The weft was made from 2 long ribbons cut in a spiral pattern in a CAM sheet that was dried over a plastic sheet. The ribbons (1.5 m) were twisted together (5 rev/cm) to form one cohesive and elastic thread. (h) The warp is tensioned in the longitudinal axis, and around, a 4.2 mm mandrel in a custom-made circular loom. The weft will be repeatedly passed between the two sets of warp ribbons to form a plain weave as described previously [29].

punctures in a hemodialysis context. The twisting aims to produce an elastic thread.

The weft is repeatedly slipped between a movable and a fixed set of tensioned warp threads to produce a vascular graft with a homogeneous wall (figure 1(h)). Modified weaving parameters were warp count (the total number of longitudinal ribbons), weft ribbons width (width of the 2 ribbons used to produce the weft thread) and weft tension used during TEVG weaving.

3.2. Effect of CAM sheet strength

In order to reduce the supraphysiological strength, and associated stiffness, of our first generation of woven TEVGs, we first investigated the effect of CAM sheet strength. The structural and mechanical properties of TEVGs produced from either stronger or weaker CAM sheets are presented in figure 2. Our group previously showed that the strength of CAM sheets can be adjusted with the time of culture during production [29, 31]. Here, we produced TEVGs from CAM sheets batches with either a perforation strength of 1162 ± 194 gram-force, referred as 'Strong sheets', or a perforation strength of 485 ± 93 gram-force, referred as 'Weak sheets' (figures 2(a)–(c)). A lower perforation strength was associated with thinner CAM sheets, which produced weft threads with a smaller diameter (figures 2(d) and (e)). As anticipated, when comparing the TEVGs produced from either stronger or weaker CAM sheets, a 22% decrease in weft thread diameter led to a similar increase in weft density (19%) (figure 2(f)). As expected, the 40% decrease in weft thread volume resulted in a considerable decrease of 32% in the burst pressure of TEVGs while internal diameter was kept constant, which is consistent with the loss of strength in the weaker CAM sheets (figure 2(g), suppl. figure 1(a)). More surprisingly, the decrease in wall thickness between TEVGs from stronger and weaker CAM sheets was limited to 10% (suppl. figure 1(b)).

The suture retention strength as well as the permeability of TEVGs were not significantly influenced by the strength of the CAM sheets (figures 2(h) and (i)). Altogether, these results demonstrated that using weaker CAM sheets allowed us to produce significantly less strong TEVGs while keeping high suture retention strength and low permeability. Therefore, the weaker CAM sheets were used for the rest of the studies on the modification of weaving parameters. Although we were able to reduce the supraphysiological strength of our TEVG by lowering the strength of our material, our substitute remained thick, poorly flexible, and still had a very wavy luminal surface (suppl. figure 1(c)). Therefore, we varied weaving parameters to further optimize our woven graft.

3.3. Effect of warp count

We first investigated the effect of decreasing the number of longitudinal threads (warp). The structural properties of TEVGs woven with warp counts of 51, 43 and 27 are presented in figure 3. Both macroscopic images and 3D reconstruction from μCT images of our grafts were used for analysis (figures 3(a) and (b)). A decrease in warp count gave more room for the ribbons to spread out in the circumferential direction and even allowed the weft to become visible (figures 3(c) and (d)). Quantification showed the expected decrease in circumferential warp density and an increase in warp ribbon width (figures 3(e) and (f)). When comparing the denser and looser

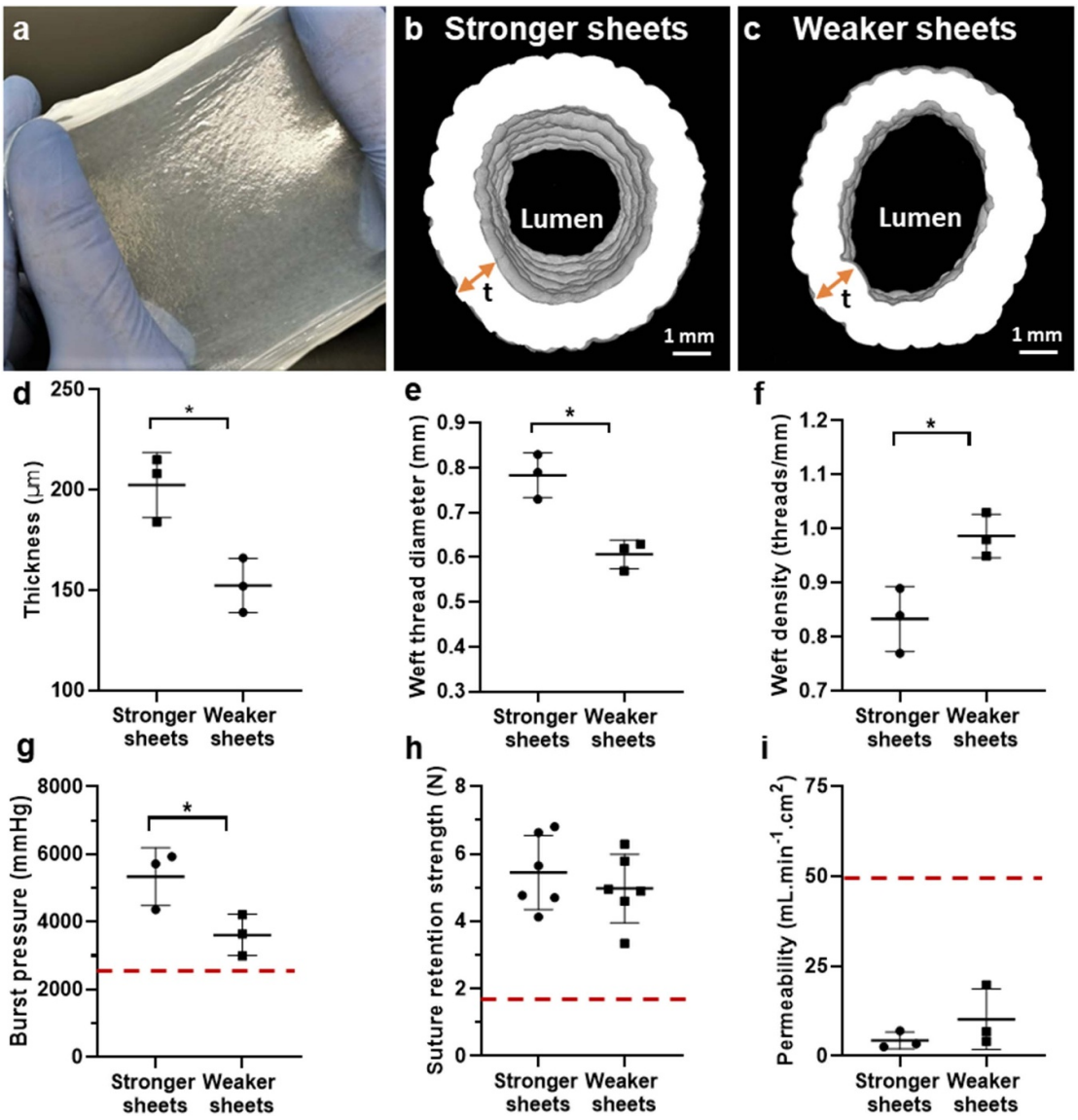

Figure 2. Structural and mechanical properties of TEVGs produced from CAM sheets with different strengths. (a) Macroscopic view of a CAM sheet. (b), (c) Representative transversal views from 3D reconstructions of TEVGs (μCT) produced from either stronger or weaker CAM sheets (t: wall thickness). (d) Thickness of CAM sheets as a function of their strength. (e) Weft thread diameter and (f) weft density in the woven TEVGs as a function of the strength of the CAM sheets. (g) Burst pressure of TEVGs produced from weaker CAM sheets decreased in comparison to the ones produced from stronger CAM sheets, while (h) suture retention strength ($n = 6$) and (i) transmural permeability were unchanged. The red dots lines represent the burst pressure (2480 mmHg) and the suture retention strength (1.8 N) of the human saphenous vein [35], and the maximal permeability (50 ml·min^{-1}·cm^{-2}) recommended for implantability [36], respectively. Results are expressed as mean ± SD, $n = 3$. * denotes $p < 0.05$ (unpaired t test and Shapiro–Wilk test).

designs, a 47% decrease in warp count led to a 28% decrease in warp density and a 36% increase in ribbon width. As expected, the more flattened warp observed with lower warp counts produced thinner walls (figures 3(g)–(i)). Lowering the warp count had the unexpected effect of reducing the vessel diameter (figures 3(g), (h) and (j)). Indeed, once removed from the 4.2 mm-mandrel of the loom and fully hydrated, the TEVGs with the lowest warp count significantly contracted. This contraction is the result of the tension that is applied to the weft during the weaving process: with more space between the warp ribbons, the stretched weft was able to pull them back together to a certain degree once removed from the mandrel.

The key mechanical properties of the TEVGs woven with different warp counts are presented in figure 4.

Burst pressure is an important indicator of graft implantability and reaching sufficient values in completely biological grafts has been a challenge for many approaches. Failure was always observed at pressures that exceeded that of human saphenous veins (2480 mmHg), a conduit routinely used for revascularization surgeries. The burst did not occur at a specific location of the TEVG, which demonstrated the homogeneity of the weaving (figures 4(a)–(c)). No significant differences in burst pressure were observed between the groups (figure 4(c)). This is consistent

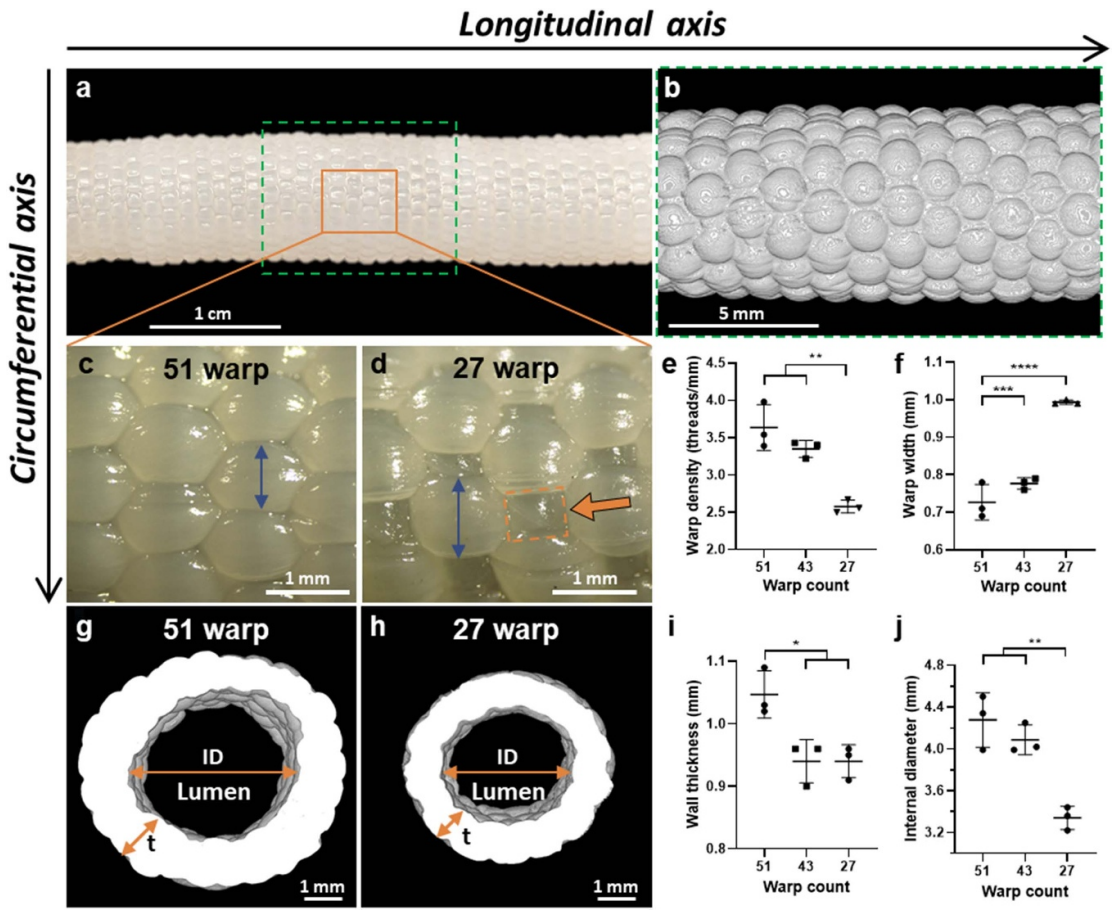

Figure 3. Structural properties of TEVGs woven with different warp counts. (a) Macroscopic side view of the graft and (b) its 3D reconstruction made from μCT images (warp count = 27). (c), (d) Closer views of the TEVG outer surface comparing 51 and 27 warp count designs. Double headed arrows point out the change in warp ribbon width and orange arrow shows the exposed weft. (e), (f) Lowering warp count led to a measurable decrease in circumferential warp density and increase in warp ribbon width. (g), (h) Representative transversal views from μCT 3D reconstructions of TEVGs woven with either 51 or 27 warp counts (*t*: wall thickness; ID: internal diameter). (i) Wall thickness but also (j) internal diameter were significantly decreased with lower warp counts. Results are expressed as mean ± SD, $n = 3$. *, **, *** and **** denotes $p < 0.05$, 0.01, 0.001 and 0.0001 respectively (one-way ANOVA and Tukey's multiple comparisons test).

with the fact that all groups had similar weft density (number of weft threads per centimeter in length) since circumferential stress is the cause of failure in burst tests (suppl. figure 2). No significant differences between the three graft designs were seen when looking at two other implantability-related properties: suture retention strength and transmural permeability (figures 4(d) and (e)). Finally, a non-statistically significant upward trend was also noted when measuring graft compliance, a property linked to long-term performance (suppl. figure 3). Overall, these results showed that lowering the warp count from 51 to 27 produced thinner-walled grafts while reducing material requirements by almost half and keeping implantability properties unchanged. Consequently, a warp count of 27 was used for the rest of the studies.

3.4. Effect of weft ribbons width

In addition to reducing the supraphysiologic strength of the vessels to bring it closer to that of native vessels, one of the objectives of this study was to lower wall thickness to make TEVGs more flexible and usable. We hypothesized both objectives could be achieved by reducing the amount of material in the weft, which supports most of the stress since circumferential stress in a tube is twice that of the longitudinal one. Hence, we produced TEVGs woven with a weft made from ribbons of narrower width: from 5 down to 4, and to 3 mm. As expected, using two 3 mm wide ribbons twisted together resulted in a weft thread with a significantly smaller diameter (figures 5(a) and (b)), which in turn resulted in TEVGs with a significantly higher weft density (≈40% increase from 5 to 3 mm) (figure 5(c)).

Moreover, this resulted in TEVGs with thinner walls, as seen on the cross sections of 3D reconstruction from μCT (figures 5(d)–(f)). However, an unforeseen effect of using a thinner weft thread was that the internal diameter of TEVGs woven increased slightly, but statistically significantly, when using a thinner thread (figures 5(d), (e) and (g)). This phenomenon is likely due to the fact that less tension was put in the weft when weaving with the more fragile thinner threads. This produced a fabric with less

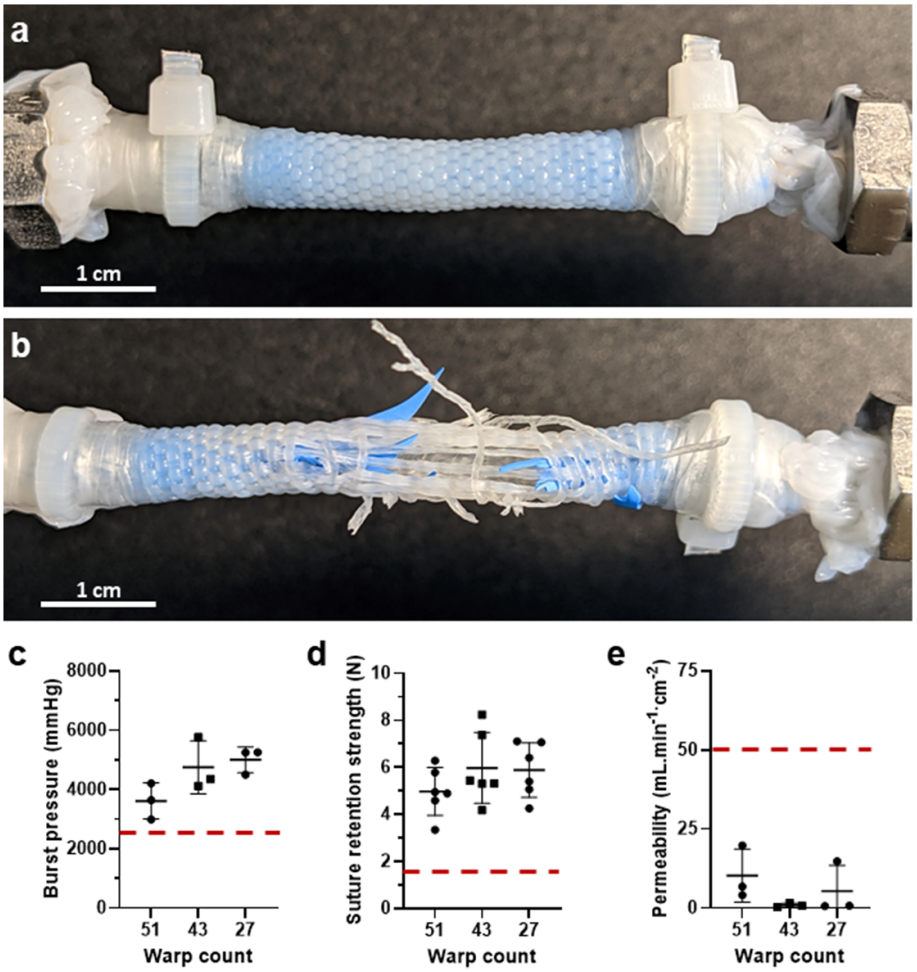

Figure 4. Mechanical properties of TEVGs woven with different warp counts. (a) Macroscopic view of a TEVG lined with a blue balloon pre-burst pressure test and (b) post-test. (c) Burst pressure, (d) suture retention strength ($n = 6$) and (e) transmural permeability of the TEVGs woven with a different number of warp threads. The red dots lines represent the burst pressure (2480 mmHg) and the suture retention strength (1.8 N) of the human saphenous vein [35], and the maximal permeability (50 ml·min^{-1}·cm^{-2}) recommended for implantability [36], respectively. Results are expressed as mean ± SD, $n = 3$ unless otherwise stated (one-way ANOVA and Tukey's multiple comparisons test).

internal tension, which did not contract as much once removed from the mandrel of the loom.

Somewhat surprisingly, despite using a weft thread that contained 40% less material, the implantability-related properties of the TEVGs did not change significantly (figure 6). This loss in material may have been compensated by the 40% increase in weft density previously shown. Suture retention strength tended to decrease with lower weft ribbons width (≈17% decrease from 5 to 3 mm), but it remained far above the suture retention strength of the human saphenous vein, a conduit commonly used in vascular surgery (figures 6(a)–(d)). Similarly, no significant differences in burst pressure and transmural permeability were observed between the different groups (figures 6(e) and (f)). The compliance tended to slightly increase when lowering weft ribbons width from 4 to 3 mm, although no significant differences were observed (suppl. figure 4). Taken together, these results showed that lowering the weft ribbons width from 5 to 3 mm reduced wall thickness and improved flexibility of the TEVGs, while keeping sufficiently strong implantability properties. Consequently, weft threads made of two 3 mm wide ribbons were used for the rest of the studies.

3.5. Effect of weft tension

The observation that some TEVGs contracted once removed from the weaving mandrel (figures 3(j) and 5(g)) led us to hypothesize that we were losing the potential elasticity of the twisted weft ribbon by completely pretensioning it during the weaving process. Since one of the objectives of this study was to improve TEVG compliance, we tested the effect of manually applying different tension levels during weaving. TEVGs were woven either loosely ('low' tension), as tightly as possible ('high'), or at an intermediary level ('medium').

When looking at the radial cross section of TEVGs woven with a high or a low tension in the weft (figures 7(a) and (b)), we can observe that a low tension during weaving significantly increased the

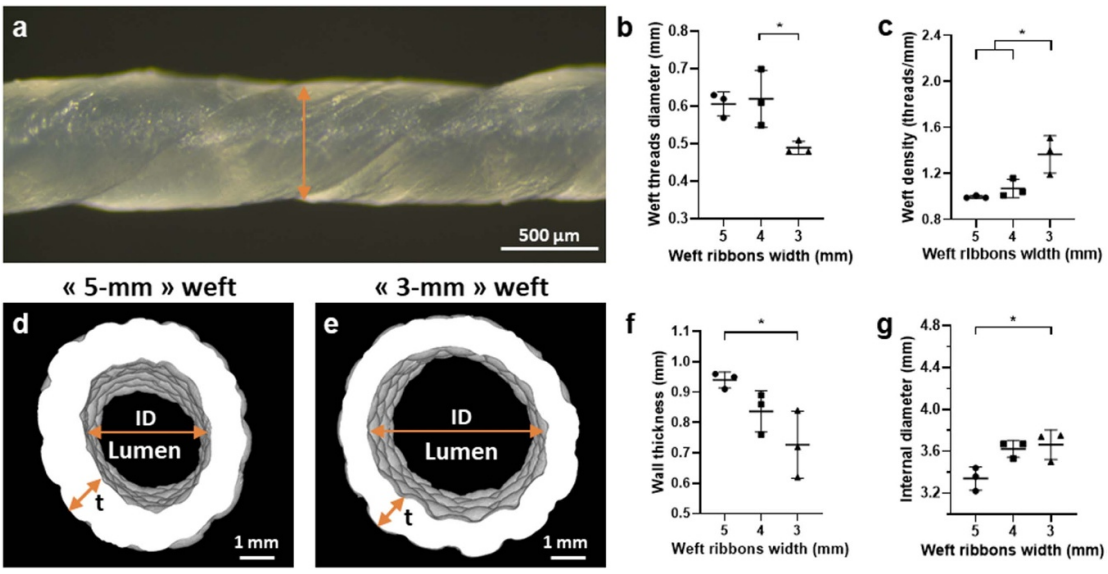

Figure 5. Influence of weft ribbons width on thread diameter and structural properties of woven TEVGs. (a) Close view of the thread used for the weft (two 5 mm wide ribbons twisted together at 5 rev/cm). (b) Weft thread diameter and (c) weft density in the woven TEVGs as a function of the width of the ribbons used. (d), (e) Representative cross sections of μCT 3D reconstructions of TEVGs woven with a weft made from two 5 mm wide ribbons and two 3 mm wide ribbons, respectively (t: wall thickness; ID: internal diameter). (f) Wall thickness and (g) internal diameter of TEVGs woven with weft of different thickness. Results are expressed as mean ± SD, $n = 3$. * denotes $p < 0.05$ (one-way ANOVA and Tukey's multiple comparisons test).

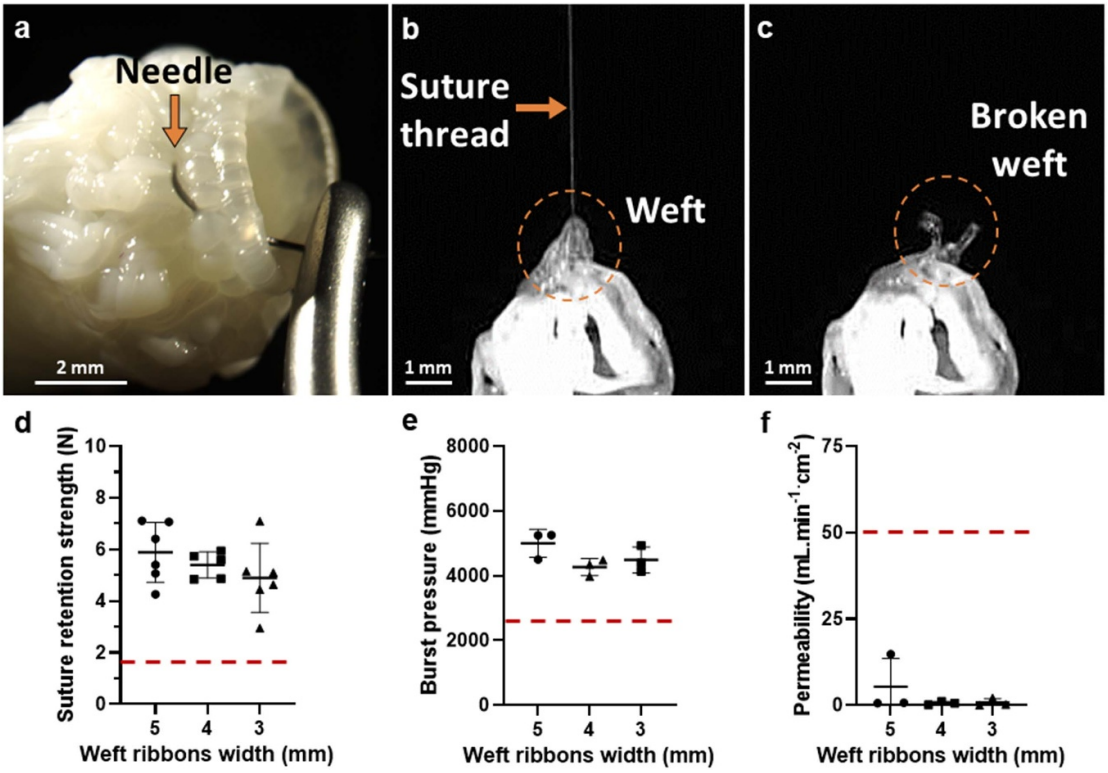

Figure 6. Mechanical properties of TEVGs woven with different weft ribbons width. (a) A single stich of 6/0 surgical suture is placed at the end of the TEVG to test the suture retention strength. (b) The suture is pulled at a constant rate until (c) failure of the weft. (d) Suture retention strength ($n = 6$), (e) burst pressure and (f) transmural permeability of the TEVGs woven with different weft ribbons width. The red dots lines represent the suture retention strength (1.8 N) and the burst pressure (2480 mmHg) of the human saphenous vein [35], and the maximal permeability (50 ml·min^{-1}·cm^{-2}) recommended for implantability [36], respectively. Results are expressed as mean ± SD, $n = 3$ unless otherwise stated (one-way ANOVA and Tukey's multiple comparisons test).

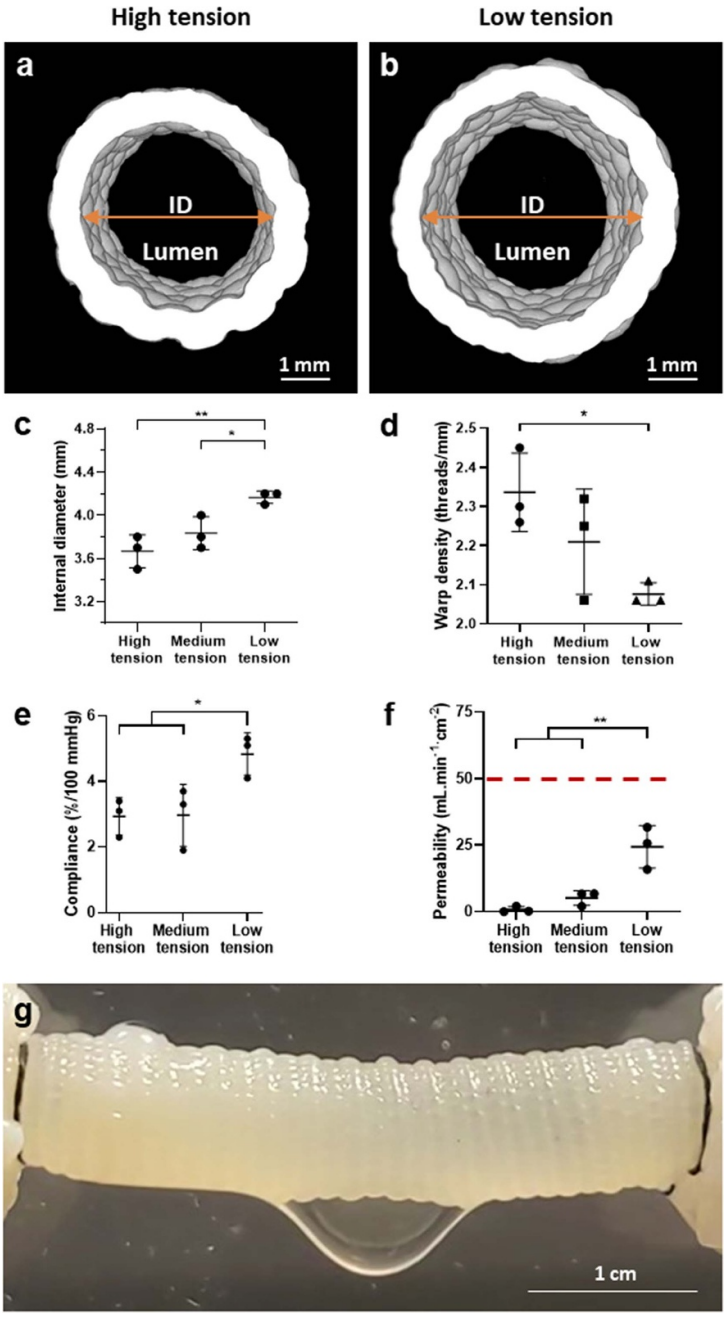

Figure 7. Influence of weft tension on the structural and mechanical properties of woven TEVGs. (a), (b) Transversal cut of 3D reconstructed woven TEVGs with (a) high tension and (b) low tension in the weft (ID: internal diameter). (c) Internal diameter and (d) warp density were significantly influenced by the tension applied to the weft. (e) Compliance and (f), (g) transmural permeability were significantly increased by a lower tension in the weft. The red dots line represents the maximal permeability (50 ml·min^{-1}·cm^{-2}) recommended for implantability [36]. Results are expressed as mean ± SD, $n = 3$. * and ** denotes $p < 0.05$ and 0.01, respectively (one-way ANOVA and Tukey's multiple comparisons test).

internal diameter in comparison to a high tension (4.2 ± 0.1 mm and 3.7 ± 0.2 mm, respectively) and decreased warp density by 9% (figures 7(c) and (d)). The fact that compliance was significantly increased with a lower tension, from 2.9% to 4.8 %/100 mmHg, supports our hypothesis (figure 7(e)). Whereas the internal diameter only increased by 13%, the compliance increased by 66%. This difference in variation supports the idea that this increase in compliance is not primarily due to the increase in diameter. As anticipated, the permeability was significantly increased in the less tightly woven TEVGs in comparison to the other groups (figures 7(f) and (g)). However, the value (24 ± 8 ml·min^{-1}·cm^{-2}) remains way below 50 ml·min^{-1}·cm^{-2}, which is a threshold often recommended for clinical applicability [36]. Wall thickness, burst pressure and suture retention strength were not significantly changed (suppl. figures 5(a)–(c)). After this optimization process, the new TEVG displayed mechanical properties that were lower than those of the first prototype, and closer to those of native blood vessels, which are the gold standard for vascular

Table 1. Mechanical properties of optimized woven TEVG compared to native blood vessels and biological TEVGs.

TEVG	Burst pressure (mmHg)	Suture retention Strength (N)	Transmural permeability (ml min^{-1} cm^{-2})	Compliance (%/100 mmHg)
1st prototype ovine TEVG	5337 ± 851 $n = 3$	5.5 ± 1.1 $n = 6$	4.3 ± 2.3 $n = 3$	1.3 ± 0.8 $n = 3$
Optimized ovine TEVG	3492 ± 307 $n = 3$ ($p < 0.05$)[a]	4.8 ± 1 $n = 6$ ($p > 0.05$)[a]	24.4 ± 8 $n = 3$ ($p < 0.05$)[a]	4.8 ± 0.6 $n = 3$ ($p < 0.01$)[a]
Human internal mammary artery [33]	3196 ± 1264 $n = 16$	1.38 ± 0.50 $n = 6$	N/A	11.5 ± 3.9 $n = 7$
Human saphenous vein [35, 37]	2480 ± 470 $n = 10$	1.8 ± 0.3 $n = 10$	N/A	1.5 ± 0.4 n not specified
TEVGs produced by Niklason *et* al [13].	2914 ± 928 $n = 5$	2.10 ± 0.53 $n = 109$	N/A	–
TEVGs produced by Tranquillo *et al* [11].	3164 ± 325 $n = 6$	1.99 ± 0.56 $n = 6$	N/A	–

[a] Indicates comparison with the 1st prototype ovine TEVG. '-' Indicates that data that were not reported. 'N/A' indicates that measurements were not applicable.

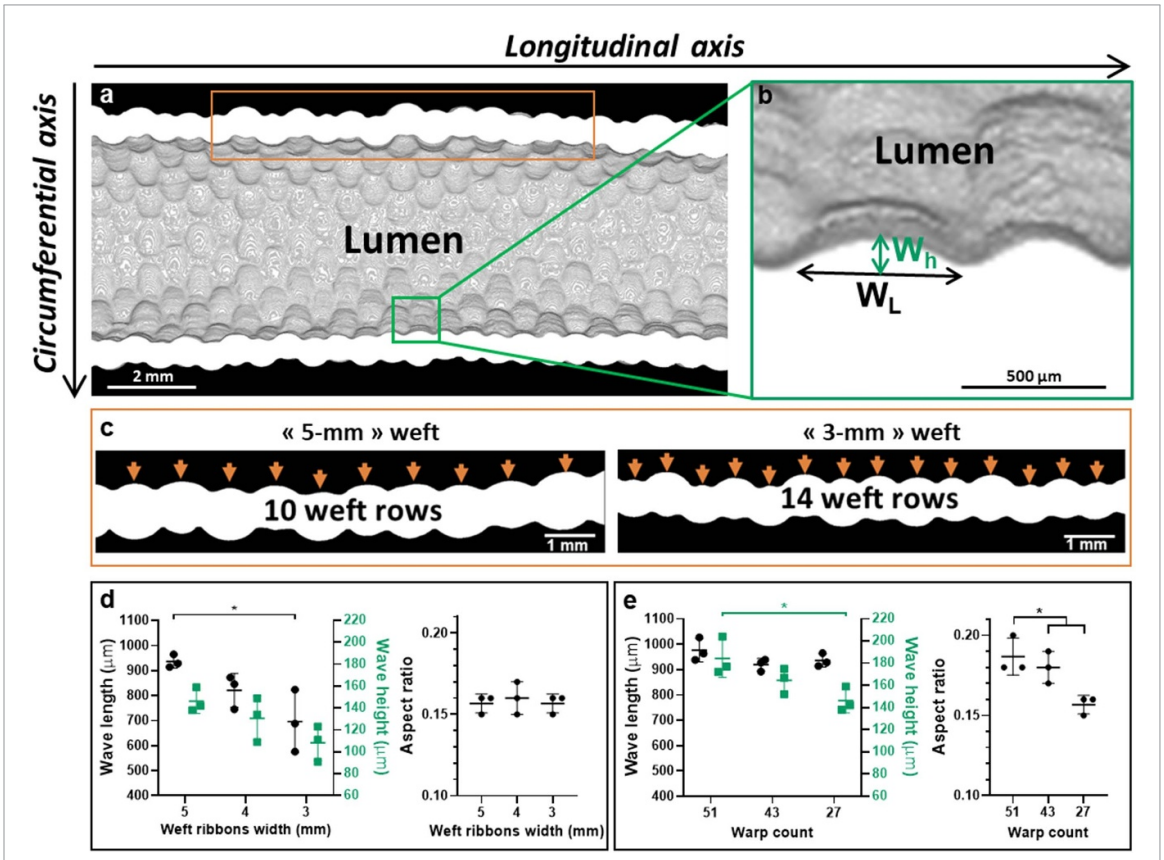

Figure 8. Effect of warp count and weft ribbons width on the luminal surface waviness of woven TEVGs. (a) Longitudinal section of a μCT 3D reconstruction of a woven TEVG with (b) a higher magnification view of the waves on the luminal surface (W_L: length of the wave; W_h: height of the wave; AR: aspect ratio). (c) Longitudinal binary images of the walls of TEVGs woven with weft made of two 5 mm wide or 3 mm wide ribbons twisted together. (d) Effect of the weft size on the waviness of the luminal surface (warp count: 27). (e) Effect of the warp count on the waviness of the luminal surface (weft: 5 mm wide ribbons). Results are expressed as mean $\pm$ SD, $n = 3$. * $p < 0.05$ (one-way ANOVA and Tukey's multiple comparisons test).

reconstruction (table 1). Moreover, a greater flexibility of the TEVG was noticeable when handling it.

3.6. Lumen surface waviness

Since we aimed to produce a vascular graft with a surface that would minimize blood flow disturbance, the effects of weaving parameters on the surface waviness were of particular interest. Longitudinal cross sections of the walls of the TEVGs show the surface profile of the luminal surface (figure 8(a)). We quantified the waviness of our samples by measuring the mean length and height of the waves (figure 8(b)). We used the aspect ratio (height over length) to quantify the steepness of the wave. When we used

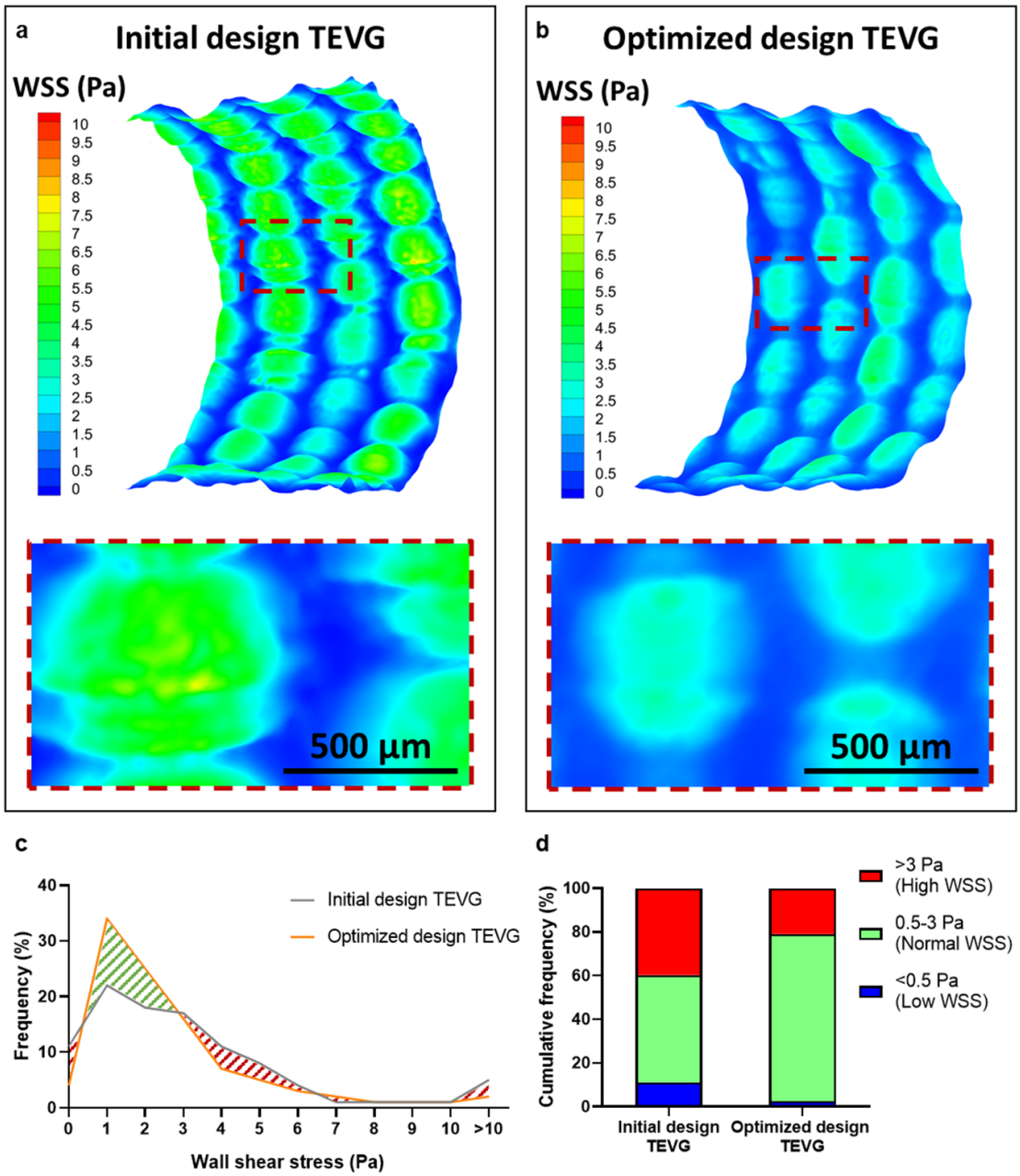

Figure 9. Effect of luminal surface waviness of woven TEVGs on wall shear stress (WSS) simulation. (a), (b) CFD simulation of WSS distribution in representative 3D reconstructions of woven TEVGs made from (a) the first design and (b) the optimized design. (c) Frequency of WSS values in TEVGs made according to the initial or optimized design. The green hashed zone represents the difference in WSS frequency in the range of normal WSS (0.5–3 Pa); the red hashed zones represent the difference in WSS frequency in the range of low (<0.5 Pa) and high WSS (>3 Pa). (d) Cumulative frequency of WSS values over low, normal, and high WSS ranges for both models.

a thinner weft ribbon, we saw that we produced a thinner wall with a higher weft density (figures 5(c) and (f)). In figure 8(c), we can visualize these effects. Quantification of the waviness revealed that using a thinner weft also reduced the length and the height, but not the aspect ratio, of the waves (figure 8(d)). However, we can see that using a lower warp count reduced the height and the aspect ratio, but not the length, of the waves (figure 8(e)). Neither the strength of CAM sheets nor weft tension had a significant effect of the waviness of woven TEVGs (suppl. figure 1(c) and suppl. figure 6).

3.7. CFD simulations of blood flow

Next, we wanted to evaluate the effect of changes in weaving design on WSS. Representative CFD models were made from μCT images of the TEVGs from our initial weaving design (warp count: 51, weft size: 2 × 5 mm wide ribbons, weft tension: high) and from grafts with the optimized weaving design (warp count: 27, weft size: 2 × 3 mm wide ribbons, weft tension: low) to simulate blood flow within the grafts (figures 9(a) and (b)). These models predicted that peak shear stress will be generated at the top of the waves with much lower WSS in the valleys between

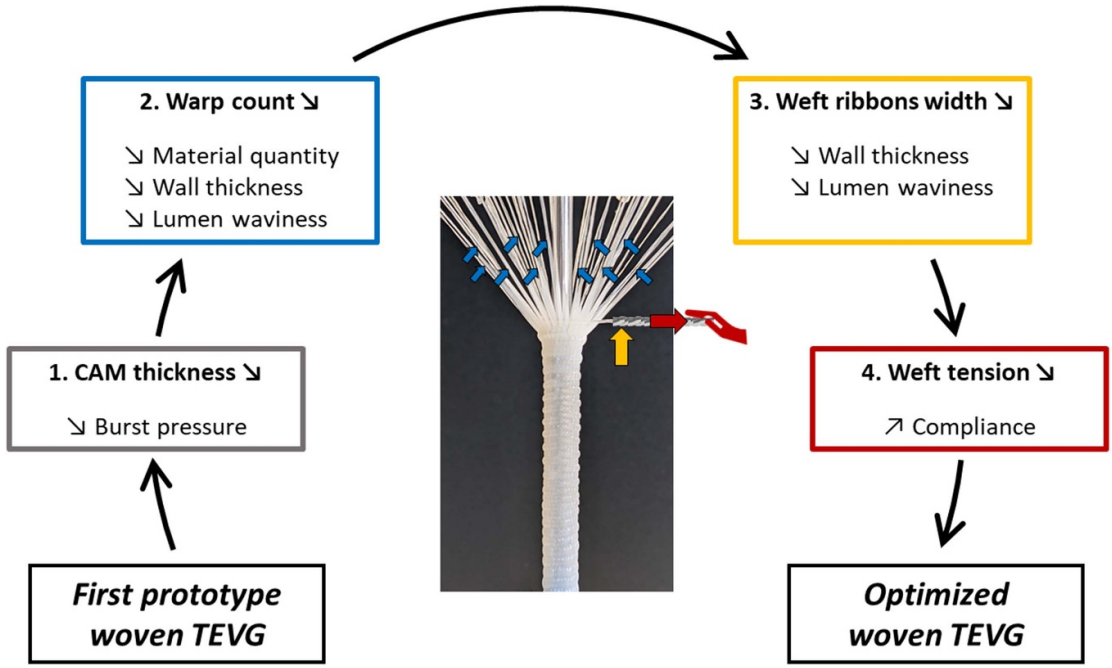

Figure 10. Overview of the effect of weaving parameters on the TEVG properties.

the weft threads. These models also indicated that the optimized design will generate lower peak shear stress as well as a more homogenous WSS. Quantification of WSS value frequencies confirmed these observations as it revealed that intermediate values were more common on the optimized surface while extreme values were rarer (figure 9(c)). Cumulative frequencies of WSS values were calculated over three ranges: low (<0.5 Pa), normal (0.5–3 Pa) and high (>3 Pa) WSS (figure 9(d)). The results showed higher frequency over the normal WSS range for the TEVG with the optimized design, with a frequency reduction of 19% and 8% in the high and low WSS ranges respectively.

3.8. Overview of the effect of weaving parameters on TEVG properties

Figure 10 summarizes what was learned about the effect of weaving parameters on the TEVG properties.

3.9. Effect of the decellularization process

In this study, all experiments were performed with 'devitalized' CAM (see method section). While previous data suggest that allogeneic 'devitalized' CAM will be well-tolerated, we wanted to study the effect of the decellularization process on the mechanical properties of woven TEVGs in case this type of popular ECM treatment would become relevant [32, 38]. Figure 11 shows the comparison between the properties of woven TEVGs from devitalized or decellularized CAM sheets. DAPI staining and DNA quantification confirmed the effectiveness of the decellularization process of the CAM sheets (figures 11(a)–(c)). DNA content was reduced by 97% to 86 ± 34 ng mg^{-1} dry CAM. Uniaxial tensile test results showed that decellularized ribbons had a slightly lower force at failure (−13%) than devitalized ribbons (figure 11(d)). The weft threads made from decellularized ribbons had a significantly smaller diameter than weft threads made from devitalized ribbons (figure 11(e)), which, consistent with earlier results (figure 8(d)), produced a significant decrease in surface waviness (suppl. figure 7(a)). The weave of devitalized TEVGs had visibly wider warp thread and appeared to have a less dense weft than decellularized grafts (figures 11(f) and (g), respectively). This observation was confirmed by a 62% increase in weft density (figure 11(h)) and a more modest, but significant, decrease in warp density of 10% (figure 11(i)) when TEVGs were decellularized. Decellularized grafts also had a slightly smaller internal diameter (7%) but a much thinner (35%) wall (suppl. figures 7(b) and (c)). The most important difference between devitalized and decellularized TEVGs was the much higher transmural permeability (288%) of decellularized TEVGs (figure 9(j)). Decellularized TEVGs had a significant higher burst pressure (96%) but unchanged suture retention strength compared to devitalized TEVGs (figures 11(k) and (l)). Finally, consistent with the increased burst pressure, the decellularized TEVGs had a significantly lower compliance (figure 11(m)).

4. Discussion

Mechanical mismatch between a vascular graft and the host artery is considered as an important cause of intimal hyperplasia, which is a major cause of graft failure [21, 23–26, 39]. Our group recently published

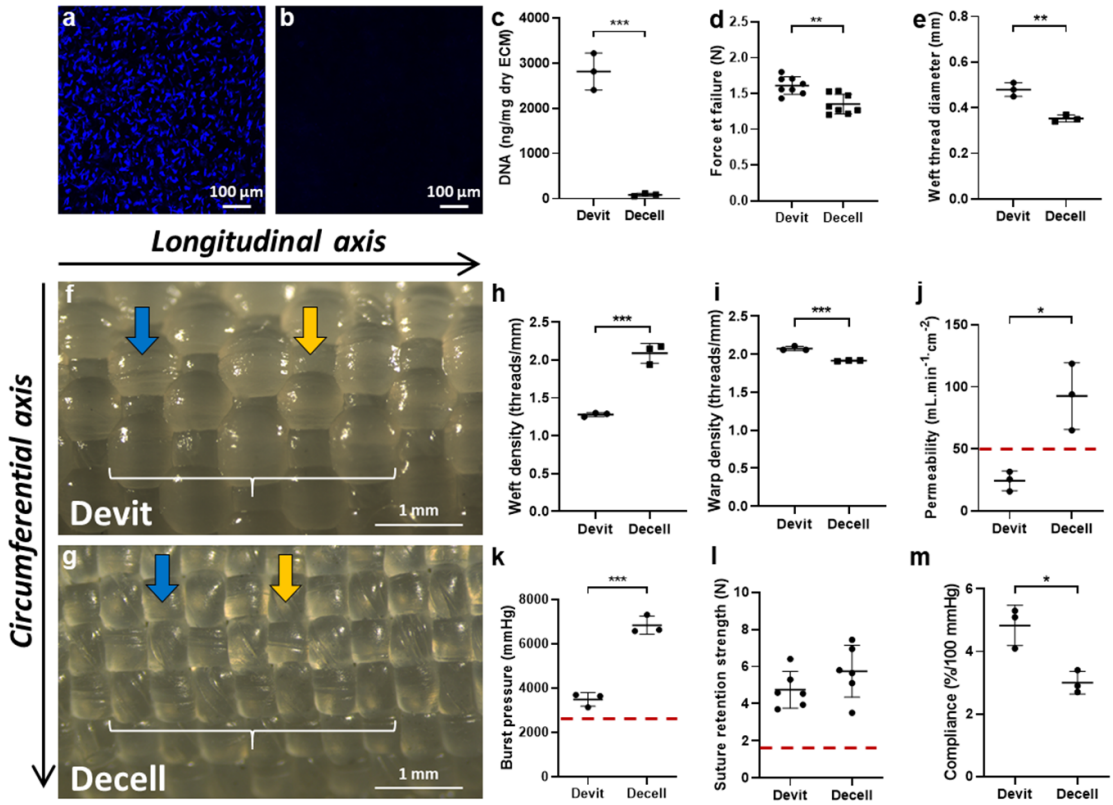

Figure 11. Decellularization of CAM sheets and mechanical properties of woven TEVGs. (a), (b) DAPI staining of (a) devitalized and (b) decellularized CAM sheets, confirmed by (c) DNA quantification. (d) Force at failure of devitalized and decellularized threads ($n = 6$, one representative experiment out of three). (e) Weft thread diameter as a function of devitalization or decellularization. Weaving with either (f) devitalized or (g) decellularized threads produced a homogenous wall, although (h) weft density was significantly higher in TEVGs from decellularized CAM, as shown by brackets of equal length. The blue arrows show a warp thread whereas the yellows arrows show the weft in both TEVGs. Devit: devitalized, Decell: decellularized. (i) Warp density was slightly but significantly decreased in decellularized TEVGs. (j) A much higher permeability was observed in decellularized TEVGs. (k) Burst pressure of decellularized TEVGs increased in comparison to devitalized ones, while (l) suture retention strength ($n = 6$) was unchanged. (m) A much higher compliance was observed in TEVGs woven with devitalized threads. The red dots lines in (j), (k) and l represent the maximal permeability (50 ml·min^{-1}·cm^{-2}) recommended for implantability [36], the burst pressure (2480 mmHg) and suture retention strength (1.8 N) of the human saphenous vein [35], respectively. Results are expressed as mean ± SD, $n = 3$ unless otherwise stated. *, ** and *** denotes $p < 0.05$, 0.01 and 0.005, respectively (unpaired t test and Shapiro–Wilk test).

two studies in which TEVGs were woven either from CAM or human amniotic membrane threads [29, 40]. Both grafts displayed burst pressure, suture retention strength, and transmural permeability that would support implantation, but would create a mechanical mismatch with native blood vessels. In the amniotic membrane study, high transmural permeability was reduced by using wider threads [40]. In the current study, we took advantage of the versatility of textile assembly to better understand how to control the overall properties of our woven CAM-based TEVG. We investigated the effects of CAM sheet strength as well as the effects of three key weaving parameters: warp counts, weft width and weft tension during weaving. The optimized woven TEVGs with weaker CAM sheets displayed a burst pressure and a compliance closer to native blood vessels, while still having high suture retention strength and low transmural permeability. In addition, this design required only half the material originally needed. They had thinner walls, which would make them more convenient for clinical use because of their increased flexibility and easier suturability. Moreover, the lumen surface waviness was decreased to reduce high WSS regions. Finally, we demonstrated the feasibility of producing decellularized woven TEVGs with mechanical properties suitable for implantation, although the decellularization process significantly changed the overall properties of the woven substitutes.

Burst pressure, and more generally mechanical strength, is an essential property for the implantation of a vascular graft. The burst pressure of the human saphenous vein (≈2500 mmHg) is often taken as the minimum required burst pressure for vascular substitute development [35]. Surprisingly, excessive burst pressure values are not discussed in TEVGs studies, despite the fact that high burst pressure should lead to mechanical mismatch [24, 25]. Our first woven TEVGs safely withstood blood pressure once implanted, but displayed a much higher burst pressure than native blood vessels (>5000 mmHg) [29]. In this work, we effectively reduced their burst

pressure primarily by using CAM sheets with lower puncture strength. As far as weaving parameters are concerned, we did not expect the warp count to influence burst pressure since this property depends on circumferential stress, also known as the hoop stress, which should be carried by the weft thread. Nonetheless, we observed an increasing trend in burst pressure (38%). This surprising result may be linked to an unforeseen effect of decreasing the warp count. Indeed, lowering the warp count allowed for an increase compression of the warp in the circumferential direction, resulting in a smaller diameter (−23%) despite using the same support mandrel. We hypothesize that this decrease in diameter, which would reduce the circumferential stress for a given pressure, largely explains the trend of decreasing burst pressure. However, we did expect to significantly decrease the burst pressure by lowering weft ribbons width from 5 mm to 3 mm. But, since weft density concomitantly increased, it compensated for the reduced weft ribbon width, and no significant change in burst pressure was observed. Lastly, we did not expect to lower the burst pressure by lowering weft tension. Although the internal diameter increased with lower tension, this change was minor (14%) and resulted in no significant changes in burst pressure. After optimizing all the production parameters, TEVGs displayed a burst pressure in the range of human small diameter arteries (≈3500 mmHg) [33].

The transmural permeability of a vascular substitute remains an important property and 50 $ml{\cdot}min^{-1}{\cdot}cm^{-2}$ is often suggested in the literature as a threshold [36]. The permeability of our optimized woven TEVG was approximately half this value. By decreasing warp count to 27 warp threads, we decreased warp density from 3.6 to 2.6 threads per mm (−28%), without any visible effect on transmural permeability. However, when we reduced warp density from 2.3 to 2.1 threads per mm (−9%) by reducing tension in the weft thread, leakage was increased by more than 24 folds. This indicates that transmural permeability does not change progressively with warp density but rather that there is a density threshold below which it increases drastically.

Wall thickness has been shown to affect the *in vivo* remodeling of vascular substitutes. Indeed, a wall thickness closer to that of native blood vessel demonstrated better compliance and kink resistance, and led to the generation of a more native neotissue [41, 42]. Moreover, thicker walls make the substitute more challenging to handle and suture. Wall thickness of biological TEVGs is usually measured *in vitro* by analysis of histological images. Here, wall thickness of woven TEVGs was measured with μCT, which allowed us to image the TEVG without causing structural changes through dehydration and harsh chemical treatments. In this study, we showed that by mainly decreasing the warp count and weft ribbons width, we reduced wall thickness of TEVGs by 38%, from 1.12 mm down to 0.69 mm, which is similar to that of the human coronary artery [43]. In the end, we reduced the amount of material used by 60% compared with the original design. With the new design, we produced an optimized TEVG with thinner walls, which is easier to handle and suture, while drastically reducing production costs.

Although burst pressure, permeability and suture retention strength are preconditions for the implantation and short-term success of a TEVG, compliance is of importance when it comes to mid- to long-term patency [23, 25, 44]. In this study, despite the fact that a decreasing warp count or weft ribbons width produced a slightly more flexible TEVG with thinner walls, these changes only resulted in a trend of decreasing in compliance. Woven structures are inherently less compliant than knitted ones, but we chose that textile assembly method for its ability to produce leakproof walls. Nonetheless, we attempted to introduce elasticity in the circumferential direction of the graft by using a weft made from two ribbons twisted together. However, we hypothesized that the weft was prestretched when TEVG were woven with a high tension, thus cancelling its elasticity. While controlling tension in this thread was challenging since these TEVGs were handmade at this stage, we demonstrated that the compliance of the TEVGs was significantly increased by lowering weft tension. This is likely the result of preserving the elasticity in the twisted thread. Alternatively, the increase in compliance could be the result of the concomitant increase in internal diameter since properties are related. However, the internal diameter increased by only 14% while the compliance increased by 66%, suggesting that most of the change in compliance was due to a lower tension in the weft. Our final design produced a TEVG with a compliance of 4.8%/100 mmHg. This value compares favorably with the current gold standard conduits for vascular repair as it exceeds the compliance of the saphenous vein (1.5%/100 mmHg) and is closer, in comparison to our first prototype, to that of the internal mammary artery (11.5%/100 mmHg) [35, 37]. However, an important limitation is that these were short-term measurements that do not guaranty that this elastic behavior will persist. While long-term *in vitro* studies can be envisioned, their ability to predict *in vivo* results can also be limited considering that a biological tissue-engineered graft is expected to be significantly remodeled after implantation [17, 45–47].

Another intrinsic property of a woven TEVG is a wavy luminal surface. Flow oscillations and WSS are well-known for influencing cell behavior and *in vivo* remodeling [48, 49]. In particular, low shear stress zones have been correlated with the development of intimal hyperplasia [50, 51]. Sho *et al* showed that a low WSS (below 5 dynes cm^{-2}) increases intimal thickening [51]. To minimize the surface profile of our TEVG, we decreased luminal

waviness by lowering the warp count and weft ribbons width. Computational flow simulations predicted an important reduction of low shear stress areas in optimized TEVG compared to the initial design (from 11.2% to 2.5%). Additionally, simulations predicted optimized TEVG to have less high shear stress regions (superior to 30 dynes cm^{-2}), which have been shown to promote thrombosis through platelet activation [52]. Overall, the waviness of the optimized TEVG is predicted to promote a more physiological range of WSS values, which may limit intimal hyperplasia by promoting an antithrombotic endothelium [52–55]. However, it is important to note this numerical model was simplified as it assumed a steady and laminar flow and a non-pulsatile pressure. While this model did not reproduce the complex turbulent flow observed in hemodialysis access grafts, a general improvement of flow conditions would be expected nonetheless.

Our strategy relies on the production of a non-living, allogeneic, and off-the-shelf vascular graft. We have favored devitalization instead of decellularization because it is a simpler process that does not have the potential to leave toxic residues nor to denature the extracellular matrix. We have shown that devitalized CAM-based TEVGs (produced by a rolled sheet approach) did not cause any clinically detectable immune response in the context of the successful implantation of three allogeneic grafts [19]. In a more recent study, *in vivo* remodeling and inflammatory response of CAM threads have been investigated in nude rats [32]. These animals, who have a functional innate immune system, did not aggressively degrade the CAM while they rapidly destroyed a clinically-used denatured ECM. Instead, a slow remodeling with very mild inflammation was observed and mechanically sound CAM threads could even be explanted after 6 months [32]. Taken together, these studies showed that our material is well-accepted by the host despite the presence of cellular debris. Nonetheless, the active removal of these debris by decellularization could improve the performance of CAM-based products if some level of immune response was to be detected in future studies. In this study, we demonstrated that we can effectively decellularize the CAM using a CHAPS-based protocol inspired by the approach of the group of Niklason [56–58]. Decellularized CAM threads had no visible nuclei in standard histology or after DAPI staining and contained only 3% of the initial DNA. This is similar to the results of Syedain *et al* who showed that, in the case of a TEVG made by ovine fibroblasts cast in a fibrin gel, a DNA content reduced by more than 90% after decellularization did not trigger allogeneic lymphocyte activation [46]. While DNA content was slightly above the often-cited threshold of 50 ng mg^{-1} dry ECM, it is good to remember that this value was established as a 'rule of thumb' based on disparate animal studies and should not be taken as a precise nor predictive value for all applications [59].

Decellularization reduced the force at failure of CAM threads by only 13%. Such small loss of mechanical strength after decellularization been reported multiple times for various ECM-derived materials [32, 56, 60, 61]. However, decellularization substantially reduced the volume of the weft thread (44%). This is consistent with the reported removal of important quantities of ECM components such as glycosaminoglycans (GAGs) by detergent-based decellularization [57, 62–65]. A consequence of using a thinner CAM thread was that the weft density increased in decellularized TEVGs, resulting in a considerably higher burst pressure and lower compliance when compared to devitalized grafts. Moreover, this decrease in thread volume led to a reduced warp density, which resulted in much more permeable TEVGs. These results demonstrate that producing a decellularized CAM-based TEVG with clinically relevant mechanical properties is possible, but further optimization of the weaving design would be needed to develop such a graft. However, these results also show that decellularization drastically affects CAM properties, which suggests that the process can partly denature the ECM as reported by others [60, 64, 65]. For now, we will continue to use devitalized CAM unless convincing evidence suggest that this material causes an immune reaction or if regulatory requirements demand it.

Zhang *et al* is the only other group that produced a completely biological TEVG using a textile approach. Their strategy relied on the use of chemically-extracted and crosslinked collagen in the form of threads that were knitted in a tube [66]. They produced a graft with satisfactory burst pressure but which was too porous. Therefore, they added an electrospun outer shell of collagen nanofibers to limit the transmural permeability inherent to knitted fabrics. However, the fact that permeability was not determined is somewhat surprising. Moreover, suture retention strength of these grafts was too low for implantation, with or without the added outer layer. To overcome this lack of mechanical strength, they had to resort to introducing biodegradable synthetic polymer threads in their constructs [10]. While theses grafts displayed burst pressure and suture retention strength appropriate for implantability, the chemically modified collagen and the synthetic polymers will have limited biological functions and will be aggressively degraded by the host. Thus, this approach will depend on the ability of the patient's body to regenerate rapidly a new blood vessel to avoid the mechanical failure of the graft. One of the important challenges of such approaches is that the balance between degradation, inflammation, and regeneration can depend on patient age, health, and other unknown factors. One of the advantages of the CAM-based approach is that it provides a large window for the host to achieve the needed remodeling of the graft.

5. Conclusion

In this study, we developed an optimized weaving design to produce a completely biological and ovine TEVG with improved structural and mechanical properties in comparison to our first prototype. By better understanding the relationship between weaving parameters and graft properties, we have created a knowledge base that will support the development of woven TEVGs or other CAM-based textiles. In particular, this toolbox could be used to adjust the graft design in view of *in vivo* performance. The next step will be to implant this optimized ovine TEVG as an allogeneic arteriovenous shunt to study its remodeling and performance in a mechanical and immunological context mimicking our clinical strategy.

Data availability statement

All data that support the findings of this study are included within the article (and any supplementary files).

Acknowledgments

This work was supported by the European Research Council (Advanced Grant #785908). We thank Grégory Hauss from *Placamat* for his technical help and acquisitions with μCT imaging. We also thank the Heart rhythm disease institute of Bordeaux (Liryc) for the collect of ovine skin biopsies obtained from post-mortem sheep.

Conflict of interest

Authors declare that they have no competing financial interests.

ORCID iDs

Gaëtan Roudier https://orcid.org/0000-0003-1082-8787
Marie Hourques https://orcid.org/0000-0001-8309-4046
Nicolas L'Heureux https://orcid.org/0000-0001-8602-3948

References

[1] Klinkert P, Post P N, Breslau P J and van Bockel J H 2004 Saphenous vein versus PTFE for above-knee femoropopliteal bypass. A review of the literature *Eur. J. Vasc. Endovasc. Surg.* **27** 357–62
[2] Rotmans J I, Heyligers J M M, Stroes E S G, Pasterkamp G and Verma S 2006 Endothelial progenitor cell-seeded grafts: rash and risky *Can. J. Cardiol.* **22** 1113–6
[3] Sayers R D, Raptis S, Berce M and Miller J H 1998 Long-term results of femorotibial bypass with vein or polytetrafluoroethylene *Br. J. Surg.* **85** 137
[4] Weinberg C B and Bell E 1986 A blood vessel model constructed from collagen and cultured vascular cells *Science* **231** 397–400
[5] Kimicata M, Swamykumar P and Fisher J P 2020 Extracellular matrix for small-diameter vascular grafts *Tissue Eng.* A **26** 1388–401
[6] Moore M J, Tan R P, Yang N, Rnjak-kovacina J and Wise S G 2022 Bioengineering artificial blood vessels from natural materials *Trends Biotechnol.* **40** 1–15
[7] Hussey G S, Dziki J L and Badylak S F 2018 Extracellular matrix-based materials for regenerative medicine *Nat. Rev. Mater.* **3** 159–73
[8] Goldstein J D, Tria A J, Zawadsky J P, Kato Y P, Christiansen D and Silver F H 1989 Development of a reconstituted collagen tendon prosthesis. A preliminary implantation study *J. Bone Jt. Surg.* **71** 1183–91
[9] Law J K, Parsons J R, Silver F H and Weiss A B 1989 An evaluation of purified reconstituted type I collagen fibers *J. Biomed. Mater. Res.* **23** 961–77
[10] Zhang F, Bambharoliya T, Xie Y, Liu L, Celik H, Wang L, Akkus O and King M W 2021 A hybrid vascular graft harnessing the superior mechanical properties of synthetic fibers and the biological performance of collagen filaments *Mater. Sci. Eng.* C **118** 111418
[11] Syedain Z H, Graham M L, Dunn T B, O'Brien T, Johnson S L, Schumacher R J and Tranquillo R T 2017 A completely biological " off-the-shelf " arteriovenous graft that recellularizes in baboons *Sci. Transl. Med.* **9** eaan4209
[12] Motta S E *et al* 2019 Human cell-derived tissue-engineered heart valve with integrated Valsalva sinuses: towards native-like transcatheter pulmonary valve replacements *npj Regen. Med.* **4** 14
[13] Lawson J H *et al* 2016 Bioengineered human acellular vessels for dialysis access in patients with end-stage renal disease: two phase 2 single-arm trials *Lancet* **387** 2026–34
[14] Gutowski P *et al* 2022 Six-year outcomes of a phase II study of human-tissue engineered blood vessels for peripheral arterial bypass *JVS-Vasc. Sci.* **4** 100092
[15] Jakimowicz T, Przywara S, Turek J, Pilgrim A, Macech M, Zapotoczny N, Zubilewicz T, Lawson J H and Niklason L E 2022 Five year outcomes in patients with end stage renal disease who received a bioengineered human acellular vessel for dialysis access *EJVES Vasc. Forum* **54** 58–63
[16] Kirkton R D, Santiago-Maysonet M, Lawson J H, Tente W E, Dahl S L M, Niklason L E and Prichard H L 2019 Bioengineered human acellular vessels recellularize and evolve into living blood vessels after human implantation *Sci. Transl. Med.* **11** 1–11
[17] L'Heureux N *et al* 2006 Human tissue-engineered blood vessels for adult arterial revascularization *Nat. Med.* **12** 361–5
[18] L'Heureux N, Pâquet S, Labbé R, Germain L and Auger F A 1998 A completely biological tissue-engineered human blood vessel *FASEB J.* **12** 47–56
[19] Wystrychowski W, McAllister T N, Zagalski K, Dusserre N, Cierpka L and L'Heureux N 2014 First human use of an allogeneic tissue-engineered vascular graft for hemodialysis access *J. Vasc. Surg.* **60** 1353–7
[20] McAllister T N *et al* 2009 Effectiveness of haemodialysis access with an autologous tissue-engineered vascular graft: a multicentre cohort study *Lancet* **373** 1440–6
[21] Post A, Diaz-Rodriguez P, Balouch B, Paulsen S, Wu S, Miller J, Hahn M and Cosgriff-Hernandez E 2019 Elucidating the role of graft compliance mismatch on intimal hyperplasia using an ex vivo organ culture model *Acta Biomater.* **89** 84–94
[22] Jeong Y, Yao Y and Yim E K F 2020 Current understanding of intimal hyperplasia and effect of compliance in synthetic small diameter vascular grafts *Biomater. Sci.* **8** 4383–95
[23] Abbott W M, Megerman J, Hasson J E, L'Italien G and Warnock D F 1987 Effect of compliance mismatch on vascular graft patency *J. Vasc. Surg.* **5** 376–82

[24] Ballyk P D, Walsh C and Butany J 1997 Compliance mismatch may promote graft–artery intimal hyperplasia by altering suture-line stresses *J. Biomech.* **31** 229–37
[25] Kidson I G 1983 The effect of wall mechanical properties on patency of arterial grafts *Ann. R. Coll. Surg. Engl.* **65** 24–29
[26] Trubel W, Schima H, Moritz A, Raderer F, Windisch A, Ullrich R, Windberger U, Losert U and Polterauer P 1995 Compliance mismatch and formation of distal anastomotic intimal hyperplasia in externally stiffened and lumen-adapted venous grafts *Eur. J. Vasc. Endovasc. Surg.* **10** 415–23
[27] Singh C, Wong C S and Wang X 2015 Medical textiles as vascular implants and their success to mimic natural arteries *J. Funct. Biomater.* **6** 500–25
[28] Akbari M, Tamayol A, Bagherifard S, Serex L, Mostafalu P, Faramarzi N, Mohammadi M H and Khademhosseini A 2016 Textile technologies and tissue engineering: a path toward organ weaving *Adv. Healthcare Mater.* **5** 751–66
[29] Magnan L *et al* 2020 Human textiles: a cell-synthesized yarn as a truly "bio" material for tissue engineering applications *Acta Biomater.* **105** 111–20
[30] Potart D, Gluais M, Gaubert A, Da Silva N, Hourques M, Sarrazin M, Izotte J, Mora Charrot L and L'Heureux N 2023 The cell-assembled extracellular matrix: a focus on the storage stability and terminal sterilization of this human " bio " material *Acta Biomater.* **166** 133–46
[31] Torres Y, Gluais M, Da Silva N, Rey S, Grémare A, Magnan L, Kawecki F and L'Heureux N 2021 Cell-assembled extracellular matrix (CAM) sheet production: translation from using human to large animal cells *J. Tissue Eng.* **12** 1–14
[32] Magnan L, Kawecki F, Labrunie G, Gluais M, Izotte J, Marais S, Foulc M-P, Lafourcade M and L'Heureux N 2021 *In vivo* remodeling of human cell-assembled extracellular matrix yarns *Biomaterials* **273** 120815
[33] Konig G *et al* 2009 Mechanical properties of completely autologous human tissue engineered blood vessels compared to human saphenous vein and mammary artery *Biomaterials* **30** 1542–50
[34] Sprenger L, Dutz S, Schneider T, Odenbach S and Hafeli U O 2015 Simulation and experimental determination of the online separation of blood components with the help of microfluidic cascading spirals *Biomicrofluidics* **9** 1–15
[35] Schaner P J, Martin N D, Tulenko T N, Shapiro I M, Tarola N A, Leichter R F, Carabasi R A and DiMuzio P J 2004 Decellularized vein as a potential scaffold for vascular tissue engineering *J. Vasc. Surg.* **40** 146–53
[36] Jonas R A, Schoen F J, Levy R J and Castaneda A R 1986 Biological sealants and knitted dacron: porosity and histological comparisons of vascular graft materials with and without collagen and fibrin glue pretreatments *Ann. Thorac. Surg.* **41** 657–63
[37] Tai N R, Salacinski H J, Edwards A, Hamilton G and Seifalian A M 2000 Compliance properties of conduits used in vascular reconstruction *Br. J. Surg.* **87** 1516–24
[38] Wystrychowski W, Cierpka L, Zagalski K, Garrido S, Dusserre N, Radochonski S, McAllister T N and L'Heureux N 2011 Case study: first implantation of a frozen, devitalized tissue-engineered vascular graft for urgent hemodialysis access *J. Vasc. Access* **12** 67–70
[39] Furdella K J, Higuchi S, Behrangzade A, Kim K, Wagner W R and Vande Geest J P 2021 *In-vivo* assessment of a tissue engineered vascular graft computationally optimized for target vessel compliance *Acta Biomater.* **123** 298–311
[40] Grémare A *et al* 2022 Development of a vascular substitute produced by weaving yarn made from human amniotic membrane *Biofabrication* **14** 045010
[41] Wu Y-L *et al* 2021 Electrospun tissue-engineered arterial graft thickness affects long-term composition and mechanics *Tissue Eng.* A **27** 593–603
[42] Johnson R, Ding Y, Nagiah N, Monnet E and Tan W 2019 Coaxially-structured fibres with tailored material properties for vascular graft implant *Mater. Sci. Eng.* C **97** 1–11
[43] Fayad Z A, Fuster V, Fallon J T, Jayasundera T, Worthley S G, Helft G, Aguinaldo J G, Badimon J J and Sharma S K 2000 Noninvasive *in vivo* human coronary artery lumen and wall imaging using black-blood magnetic resonance imaging *Circulation* **102** 506–10
[44] Walden R, L'italien G J, Megerman J and Abbott W M 1980 Matched elastic properties and successful arterial grafting *Arch. Surg.* **115** 1166–9
[45] Blum K M *et al* 2022 Tissue engineered vascular grafts transform into autologous neovessels capable of native function and growth *Commun. Med.* **2** 1–21
[46] Syedain Z H, Meier L A, Lahti M T, Johnson S L and Tranquillo R T 2014 Implantation of completely biological engineered grafts following decellularization into the sheep femoral artery *Tissue Eng.* A **20** 1726–34
[47] Breuer T, Jimenez M, Humphrey J D, Shinoka T and Breuer C K 2023 Tissue engineering of vascular grafts: a case report from bench to bedside and back *Arterioscler. Thromb. Vasc. Biol.* **43** 399–409
[48] Motta S E *et al* 2020 Geometry influences inflammatory host cell response and remodeling in tissue-engineered heart valves *in-vivo Sci. Rep.* **10** 1–15
[49] van Haaften E E, Quicken S, Huberts W, Bouten C V C and Kurniawan N A 2021 Computationally guided *in-vitro* vascular growth model reveals causal link between flow oscillations and disorganized neotissue *Commun. Biol.* **4** 546
[50] Zarins C K, Giddens D P, Bharadvaj B K, Sottiurai V S, Mabon R F and Glagov S 1983 Carotid bifurcation atherosclerosis. Quantitative correlation of plaque localization with flow velocity profiles and wall shear stress *Circ. Res.* **53** 502–14
[51] Sho E, Nanjo H, Sho M, Kobayashi M, Komatsu M, Kawamura K, Xu C, Zarins C K and Masuda H 2004 Arterial enlargement, tortuosity, and intimal thickening in response to sequential exposure to high and low wall shear stress *J. Vasc. Surg.* **39** 601–12
[52] Hathcock J J 2006 Flow effects on coagulation and thrombosis *Arterioscler. Thromb. Vasc. Biol.* **26** 1729–37
[53] Byrom M J, Bannon P G, White G H and Ng M K C 2010 Animal models for the assessment of novel vascular conduits *J. Vasc. Surg.* **52** 176–95
[54] Baeyens N *et al* 2015 Vascular remodeling is governed by a VEGFR3-dependent fluid shear stress set point *eLife* **2015** 1–35
[55] Dolan J M, Meng H, Singh S, Paluch R and Kolega J 2011 High fluid shear stress and spatial shear stress gradients affect endothelial proliferation, survival, and alignment *Ann. Biomed. Eng.* **39** 1620–31
[56] Gui L, Muto A, Chan S A, Breuer C K and Niklason L E 2009 Development of decellularized human umbilical arteries as small-diameter vascular grafts *Tissue Eng.* A **15** 2665–76
[57] Dahl S L M *et al* 2011 Readily available tissue-engineered vascular grafts *Sci. Transl. Med.* **3** 68ra9
[58] Prichard H L, Manson R J, DiBernardo L, Niklason L E, Lawson J H and Dahl S L M 2011 An early study on the mechanisms that allow tissue-engineered vascular grafts to resist intimal hyperplasia *J. Cardiovasc. Transl. Res.* **4** 674–82
[59] Crapo P M, Gilbert T W and Badylak S F 2011 An overview of tissue and whole organ decellularization processes *Biomaterials* **32** 3233–43
[60] Dahl S L M, Koh J, Prabhakar V and Niklason L E 2003 Decellularized native and engineered arterial scaffolds for transplantation *Cell Transplant.* **12** 659–66
[61] Narita Y, Kagami H, Matsunuma H, Murase Y, Ueda M and Ueda Y 2008 Decellularized ureter for tissue-engineered small-caliber vascular graft *J. Artif. Organs* **11** 91–99

[62] Mendoza-Novelo B, Avila E E, Cauich-Rodríguez J V, Jorge-Herrero E, Rojo F J, Guinea G V and Mata-Mata J L 2011 Decellularization of pericardial tissue and its impact on tensile viscoelasticity and glycosaminoglycan content *Acta Biomater.* **7** 1241–8
[63] Uhl F E *et al* 2020 Functional role of glycosaminoglycans in decellularized lung extracellular matrix *Acta Biomater.* **102** 231–46
[64] Petersen T *et al* 2010 Tissue-engineered lungs for *in vivo* implantation *Science* **329** 2008–11
[65] Hwang J, San B H, Turner N J, White L J, Faulk D M, Badylak S F, Li Y and Yu S M 2017 Molecular assessment of collagen denaturation in decellularized tissues using a collagen hybridizing peptide *Acta Biomater.* **53** 268–78
[66] Zhang F, Xie Y, Celik H, Akkus O, Bernacki S H and King M W 2019 Engineering small-caliber vascular grafts from collagen filaments and nanofibers with comparable mechanical properties to native vessels *Biofabrication* **11** 1173–8